Frictional Resistance within the Wake of Frictional Rupture Fronts

Ilya Svetlizky, Elsa Bayart, Gil Cohen, and Jay Fineberg
The Racah Institute of Physics, The Hebrew University of Jerusalem, Jerusalem 91904, Israel
(Received 15 March 2017; published 8 June 2017)

Frictional resistance to slip, τ, is determined by the real area of contact, A, and the shear strength of the contacts forming the frictional interface. We perform simultaneous high-speed local measurements of τ and A at the tail of propagating rupture fronts. Rate dependence is investigated over 2 orders of magnitude of local slip velocities which reach up to ~ 1 m/s. A critical slip velocity is observed that signifies a transition in the frictional behavior: enhanced velocity weakening of A and τ. These measurements enable us to infer the contact shear strength, an otherwise elusive quantity, and show that the contact shear strength persistently increases with slip rate. This, surprisingly, contrasts with expected contact softening at the high temperatures induced by rapid sliding.

DOI: 10.1103/PhysRevLett.118.234301

The real area of contact formed by two rough surfaces is substantially smaller than the ostensible contact area, as it is composed of a myriad of discrete microscopic contacts [1,2]. The pressure at these contacts is therefore huge, often reaching material yield stresses. The mechanical properties of the frictional interface consequently differ significantly from those of the elastic bulk material. Although critically important, direct measurement of interface properties is elusive, as they are hidden within the microscopically thin frictional interface. Two of these, the real area of contact and the contact shear strength, determine the frictional resistance to sliding [3]. These are crucial for our fundamental understanding of friction and directly impact applications ranging from the sliding of everyday macroscopic objects to the relative motion of tectonic plates.

The frictional resistance of sliding bodies is commonly represented by an effective single degree of freedom, the "dynamic friction coefficient" in experiments where the sliding velocities, v, are externally imposed with values $0.01\,\mu\mathrm{m/s} < v < \sim 1\,\mathrm{m/s}$. In such experiments, friction commonly weakens logarithmically with increasing v [3–6] for slow velocities. This weakening has been interpreted as thermally activated creep [3,7–9], that often crosses over to velocity strengthening at higher slip rates [10–12]. At extreme values ($v > 0.1$ m/s) substantial weakening occurs that often (but not always [13]) is attributed to significant temperature increase [14–18]. Extreme *local* values of v occur *naturally* in the transition to frictional motion, that occurs via dynamically propagating fronts that rupture the contacts forming the frictional interface [19]. These ruptures generate *local* slip velocities whose values often surpass the most rapid imposed v [20–26]. The stresses and material velocities at the tip of these rupture fronts are described by the singular solutions of linear elastic fracture mechanics, LEFM, that describe brittle shear cracks [22,24,27]. The rapid propagation of these singularities has impeded experimental study of frictional resistance evolution.

Here we experimentally study the frictional resistance (the local dynamic friction coefficient) in the wake of propagating rupture fronts whose propagation velocities range from a small fraction of the Rayleigh wave speed, C_R, to values that either asymptotically approach C_R or surpass the shear wave speed, C_S to reach the longitudinal speed of sound, C_L. By combining high-speed measurements of the stresses adjacent to the frictional interface, the real area of contact and sliding velocities we trace the interrelation of these dynamic quantities. We find that, surprisingly, the velocity dependence of the local frictional resistance is both nontrivial and implies that contacts persistently strengthen—even at extreme values of v.

We study the interface strength of contacting poly (methylmethacrylate) (PMMA) plates ($\rho \approx 1,170\,\mathrm{kg/m^3}$). The x, y, z dimensions of the upper plate were 200, 100, 5.5 mm [Fig. 1(a)]. Lower plates were either thin (240, 100, 5.5 mm) or thick (300, 30, 30 mm). Rayleigh, shear, and longitudinal wave speeds are, respectively, $C_R \approx 1237$ m/s, $C_S \approx 1345$ m/s, and $C_L \approx 2333$ m/s (plane stress) [24]. The system is approximately 2D with a quasi 1D frictional interface, as the 5.5 mm interface width is considerably smaller than other system dimensions. The contacting surfaces were cleaned by distilled water and isopropyl alcohol and then dried for about 2 h [28]. A high speed camera (580 000 frames/s) was used to visualize the dynamic changes in the real area of contact, $A(x,t)$, via a method of total internal reflection [19,24,32]. The entire 200 mm × 5.5 mm frictional interface was mapped to 1280 × 8 pixels; each pixel represented the sum value of a large ensemble of discrete contacts. The three components of the 2D strain tensor, $\varepsilon_{ij}(x,t)$, were continuously and simultaneously measured every 1 μs at 16–19 spatial locations at $y \approx 3.5$ mm above the interface [Fig. 1(a)]. The two plates were carefully aligned and pressed together

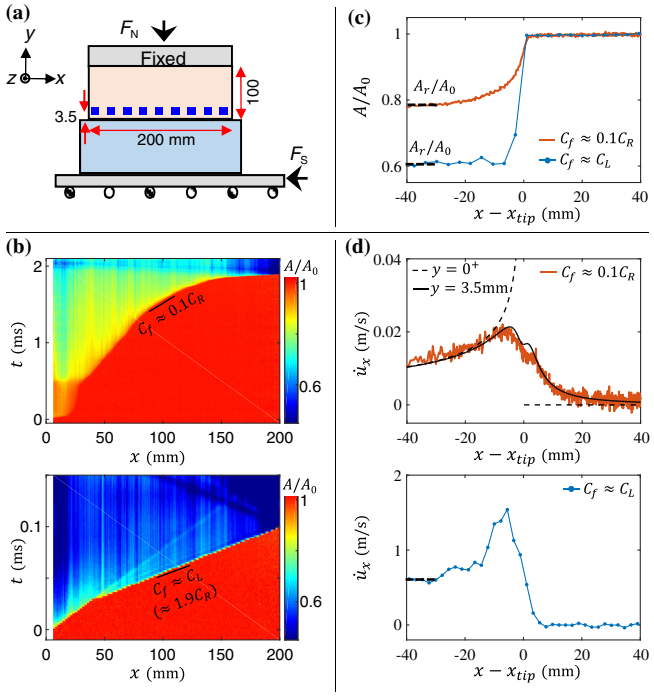

FIG. 1. Evolution of the real area of contact and material velocities during rupture front propagation. (a) Two PMMA blocks are used in a stick slip friction experiment. Rosette strain gauges, mounted within the upper plate ~3.5 mm above the frictional interface, measure all components of the 2D strain tensor every 1 μs. (b) The evolution of $A(x,t)$ for typical slow (top) and supershear (bottom) rupture fronts. The fronts nucleate at $x \approx 0$ and reduce $A(x,t)$ in their wake. (c) Reduction of A/A_0 with local rupture velocities $C_f \approx 0.1C_R$ (orange line) and $C_f \approx C_L$ (blue line). A_r denotes the residual area of contact at the tail of the propagating rupture front. (d) Material velocities, $\dot{u}_x$ at $y \approx 3.5$ mm, inferred from measured ε_{xx} [24]. (top) Slowly propagating rupture, with LEFM prediction (solid line). $\Gamma \approx 2.5$ J/m^2, the fracture energy, is the sole free parameter [24]. Dashed line is the singular velocity, $\dot{u}_x(y = 0^+)$, predicted by LEFM. At $x - x_{\rm tip} < -20$ mm measured $\dot{u}_x(y = 3.5$ mm$)$ correspond to $\dot{u}_x(y = 0^+)$. (bottom) $\dot{u}_x$ for a supershear rupture. (c),(d) Rupture tip position, $x_{\rm tip} = 110$ mm. Lower values of A_r correspond to faster $\dot{u}_x$.

by an external normal force, $F_N \approx 5,500N$ (5 MPa of nominal pressure) [Fig. 1(a)]. Afterwards, shear forces, F_S, were applied quasistatically until motion either spontaneously initiated or was externally triggered [33].

Figure 1(b) presents typical measurements of $A(x,t)$ for both sub-Rayleigh ($C_f < C_R$) and supershear ($C_f > C_S$) fronts where C_f is the rupture front velocity. The onset of frictional motion is mediated by cracklike rupture fronts that leave in their wake significantly reduced A. The boundary between regions of intact and reduced areas of contact defines the rupture tip position, $x_{\rm tip}$. In these examples, ruptures nucleated at $x \approx 0$ and accelerated in the positive x direction. Figure 1(c) describes the corresponding evolution of $A(x,t)$ at $x = 110$ mm. Temporal measurements of $A(x = 110\text{ mm}, t)$ were converted to a spatial profile $A(x - x_{\rm tip})$ by utilizing $A(x,t) = A(x - \int C_f dt)$ [24]. This method eliminated any spatial variation due to inhomogeneities along the frictional interface. Residual contact areas, A_r, were measured at times corresponding to $x - x_{\rm tip} = -35$ mm, chosen to be both beyond any dynamic variation of A associated with the rupture tip and prior to the arrival of any reflections, as seen in Fig. 1(b) for $t > 2$ ms (top) and $t > 0.1$ ms (bottom).

We now consider the slip velocity following the passage of ruptures. Figure 1(d) presents measurements of the material velocity, $\dot{u}_x$ (where u_x is the x component of the displacement field in the lab frame), at $y \approx 3.5$ mm (top plate). As for A, temporal measurements of $\dot{u}_x$ are converted to spatial profiles. Material velocities, as well as all components of stress and strain fields near the rupture tip ($C_f < C_R$), are dominated by the universal square-root singular form originally developed to describe brittle shear cracks [24,27]. Figure 1(d), top demonstrates the agreement between brittle fracture theory and measured $\dot{u}_x(y = 3.5$ mm$)$ (solid black line). For $x - x_{\rm tip} < -20$ mm measured $\dot{u}_x(y = 3.5$ mm$)$ reliably reflect the velocities at the interface $\dot{u}_x(y = 0^+)$. The relative local velocity between the plates, the slip velocity, is given by $v = 2\dot{u}_x(y = 0^+)$ as $\dot{u}_x(x,y)$ is antisymmetric with respect to y [34]. (In the case of the thin top plate on the thick bottom block, where antisymmetry does not strictly apply, we expect only small corrections to v for $C_f < 0.9C_R$ [35].) Faster ruptures are associated with larger v [Fig. 1(d)] and are accompanied by lower values of A_r [Fig. 1(c)]. In what follows, local values of v (measured simultaneously with A_r) will be systematically related to A_r and frictional resistance at the tails of propagating rupture fronts.

Figure 2(a) presents measurements of ε_{xy} at $y \approx 3.5$ mm for the two rupture events presented in Fig. 1. In order to calculate the shear stresses, σ_{xy}, the viscoelastic constitutive law for PMMA [36,37] must be used. For a viscoelastic material in the region of linear response at small strains $\sigma_{xy}(\omega) = 2\mu^*(\omega)\varepsilon_{xy}(\omega)$, where $\mu^*(\omega)$ is the frequency dependent complex shear modulus. Its real and imaginary parts are the storage and loss modulus, respectively. In our case, we neglect the loss modulus [36]. We further simplify the analysis by using the large separation of time scales between the long interevent time (~10 s) and the short times ($10 - 500$ μs) associated with the rupture passage. This yields

$$\sigma_{xy}(t) = 2\mu_f[\varepsilon_{xy}(t) - \varepsilon_{xy}^0] + 2\mu_s\varepsilon_{xy}^0, \qquad (1)$$

where $\mu_f = 2.1 \pm 3\%$ and $\mu_s = 1.2 \pm 5\%$ GPa are directly measured fast and slow storage moduli and ε_{xy}^0 are initially imposed shear strains, as denoted in Fig. 2(a). The validity of this approximation was explicitly verified. The calculated σ_{xy} are plotted in Fig. 2(b). Figure 2 demonstrates that it is important to properly account for viscoelasticity.

Residual stresses, τ_r, are measured at times corresponding to $x - x_{\rm tip} = -35$ mm, which are well beyond dynamic

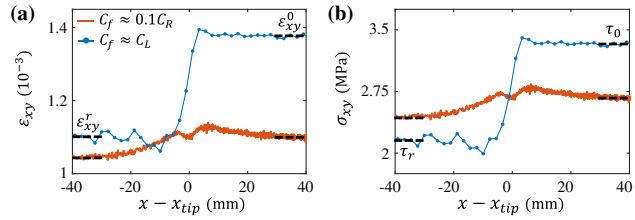

FIG. 2. Stress calculations are highly influenced by properly accounting for viscoelasticity. (a) Examples of the measured ε_{xy} plotted relative to the rupture tip position $x_{\mathrm{tip}} = 110$ mm. ε^0_{xy} is the initial strain level, prior to the rupture arrival. (b) Shear stresses, σ_{xy}, are calculated from the measured ε_{xy} by using the viscoelastic constitutive law of PMMA [Eq. (1)]. τ_r, the residual frictional resistance are measured at times corresponding to $x - x_{\mathrm{tip}} = -35$ mm beyond any dynamic stress variations associated with the rupture tip. Note that the decrease of τ_r with C_f only becomes apparent when viscoelasticity is accounted for. (a), (b) Profiles of ε_{xy} and σ_{xy} corresponding to the A/A_0 measurements in Fig. 1(c) during slow (orange line) and supershear (blue line) rupture events. Local σ_{yy} values are the same for both rupture events.

stress variations associated with the rupture tip. τ_r, therefore, represent the local frictional resistance during sliding due to the nonzero value of A_r after the rupture passage [Fig. 1(c)]. To first order the values of τ_r scale linearly with the local normal stress, $\sigma_{yy}(y = 0)$, denoted from here on by σ [Fig. S1(a)], where the proportionality factor is the local dynamic friction coefficient. For a given σ, however, τ_r is not constant [Fig. 2(b)]. Here we focus on the (second order) rate dependence of τ_r. The difference $\Delta\tau = \tau_0 - \tau_r$ provides a measure of the amount of released elastic energy and plays a key role in both rupture dynamics [33] and rupture arrest [38,39].

In Fig. 3 we consider the systematic variations of τ_r and A_r with simultaneously measured slip velocities, v. The figure is composed of multiple spatial measurements within ~30 rupture events over a wide range of C_f; $\sim 0.05C_R < C_f < \sim C_R$ (orange and green symbols) and $C_f \approx C_L$ (blue symbols). In this range of C_f, v spanned over 2 orders of magnitude. Note that for the experimental setup of a thin top plate on a thick bottom block at $C_f \to C_R$ geometrical effects result in a coupling between v and σ [35]. Therefore, in this block geometry (green symbols) only $C_f < 0.9C_R$ were considered.

The measurements in Fig. 3(a) and 3(b) reveal the existence of a critical slip velocity, v_c (~0.1 m/s), that signals a transition in the frictional behavior. For $v < v_c$, A_r decreases logarithmically with v while no significant change is observed in τ_r. For $v > v_c$, the rate of logarithmic decrease of A_r becomes ~2.5 times larger and velocity weakening of τ_r commences. If the frictional properties of the interface (τ_r and A_r) were solely dependent on the instantaneous slip velocity, then we would expect that our measurements for sub-Rayleigh (orange symbols) and supershear (blue symbols) ruptures would collapse onto the same curves. While this is approximately true, differences in the two rupture regimes are apparent in both τ_r and A_r in Fig. 3. These differences suggest a nontrivial history dependence of the frictional properties of the interface; τ_r and A_r are not solely dependent on instantaneous values of v. One would not expect this history dependence if contacts were wholly renewed during slip.

Several comments are in order. First, ~20% spatial variations of τ_r/σ (Fig. S1) are common. In Fig. 3(a) we accounted for these spatial variations by normalizing the measurements at different locations (See Sec. I in Ref. [28]). Second, the ~5% uncertainty in μ_f and μ_s values

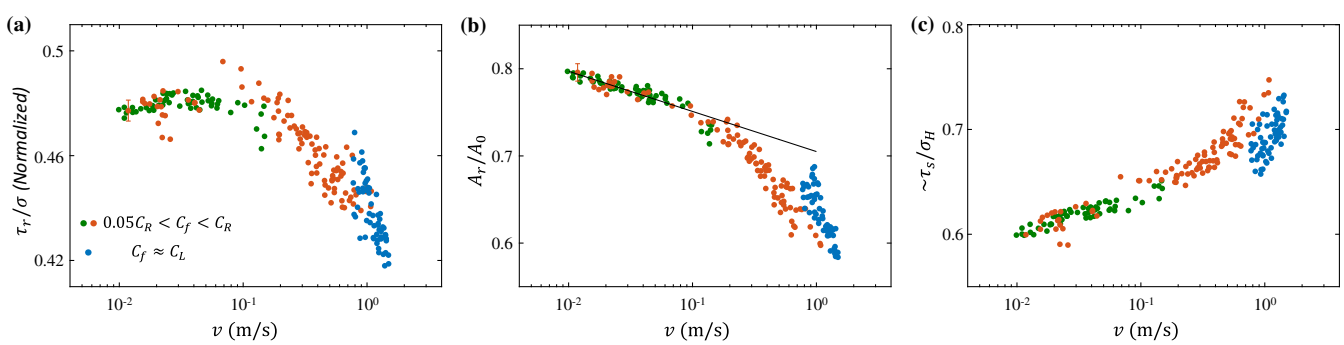

FIG. 3. Enhanced velocity weakening above a critical slip velocity, v_c. (a) Variation of the residual frictional resistance, τ_r [Fig. 2(b)], as a function of the local slip velocity [Fig. 1(d)]. τ_r weakens with increasing v for $v > v_c$ (~0.1 m/s). Values of τ_r/σ were normalized to account for spatial variations of the measurements (see Sec. I in Ref. [28]). (b) Corresponding measurements of the residual contact area, A_r/A_0 [Fig. 1(c)]. The rate of the logarithmic reduction of A_r with v increases by a factor of ~2.5 at $v > v_c$. This enhanced reduction of A_r is concurrent with the weakening of τ_r. (c) The rate dependence of the contact shear strength, τ_s, is obtained by taking the ratio of τ_r/σ and A_r/A_0. This ratio roughly scales as τ_s/σ_H, where σ_H is the material hardness. (a)–(c) Green is the thin top plate on thick bottom block. In this block geometry only $C_f < 0.9C_R$ were considered. Orange ($\sim 0.05C_R < C_f < \sim C_R$) and blue ($C_f \approx C_L$) correspond to identical geometries of the top and bottom plates; ~30 rupture events are presented. The measurements are all local measurements performed in the central region 90 mm $< x <$ 140 mm of our interfaces.

does not affect the presented rate dependence of τ_r. Third, we have explicitly verified that interevent healing times (5–15 s) result in very small variations of A_0 (<5%); therefore, the rate dependence of A_r/A_0 presented in Fig. 3(b) should be attributed to the rate dependence of A_r.

A, the local sum of the microsize contacts, is significantly smaller than the nominal contact area, A_n [40]. In the continuum limit, τ, the local frictional resistance (stress) is expected to be [1]

$$\tau = A/A_n \tau_s, \tag{2}$$

where τ_s is the shear strength per unit area of the contacts. Using Eq. (2) and the relation $A_0/A_n \sim \sigma/\sigma_H$, where σ_H is the material hardness [1,2], therefore, enables us to determine τ_s during sliding from direct measurements of τ_r/σ and A_r/A_0 by $\tau_s/\sigma_H \sim (\tau_r/\sigma)/(A_r/A_0)$. Figure 3(c) presents the rate dependence of τ_s and shows that τ_s continuously *increases* with v, despite the decreasing values of both τ_r and A_r with v.

We now consider the rate dependence of A. Generally, A exhibits nontrivial rate and history dependence which are not yet completely understood. In the rate and state framework [3], A is often described by

$$A/A_n = \sigma/\sigma_H[1 + \beta \log(1 + \phi/\phi^*)], \tag{3}$$

where ϕ is a state variable [3,4,6,11,41–43] that is typically interpreted as the "contact lifetime" and ϕ^* is a short time cutoff [3,12,44]. Setting $\phi = t$, for instance, captures the logarithmic increase of A with the contact time (aging) of two pressed materials [23,40] (Fig. S2). Furthermore, logarithmic velocity weakening of τ, observed in experiments with imposed slow slip velocities ($v < 10^2$ μm/s) [3–5], has been explained via Eq. (2) with the suggestion that A decreases due to the reduction of the contact lifetime with increasing v; $\phi \sim d_c/v$, where d_c is a typical contact size.

Figure 3(b) provides direct evidence for such a logarithmic decrease of A for *local* values of v at slow rates ($<v_c$). For $v < v_c$ we estimate β as 0.03 ± 0.01 (Sec. II in Ref. [28]). This value of β, while consistent with β measured during the aging of A (Fig. S2), is 20%–80% smaller. This observation contrasts with experiments on rock [6], where the values of β measured during aging and sliding by sound transmission across the interface were more closely comparable. Our experiments significantly differ from sliding experiments in rock, as here the slip rates are both much higher, measurements are local, and no powderlike ("gouge") layer of ground rock is formed. Our observations may suggest that the form of Eq. (3) may be too simple.

What is the origin of the transition at v_c? Rapid temperature increase (flash heating) is expected during the contact lifetime due to frictional heating at high slip rates [14]. By taking into account the generated heat ($\tau_s v$) and the heat transport away from the interface to the material bulk, this temperature increase can be estimated. These calculations imply that contact temperatures should reach the glass (~400 K) temperatures of PMMA at slip rates in the range of 0.1–1 m/s (Fig. S3), suggesting significant contact softening. This transitional slip rate is indeed consistent with the observed transition velocity, $v_c \sim 0.1$ m/s. In macroscopic sliding experiments where bulk PMMA blocks were externally heated to near their glass temperature, decreased friction was indeed observed [5]. On the other hand, we would intuitively expect that such severe softening of the contacts should be accompanied by large reductions in both τ_r and τ_s. This, remarkably, is not evident in the data; our observed reduction of τ_r is only at the level of a few percent. This highly nonintuitive result is echoed in the inferred frictional strength of the contacts τ_s, which continuously *increases* with v [Fig. 3(c)]. This increase of τ_s takes place, in contrast to τ_r, both below and above v_c. While logarithmic velocity strengthening of τ_s for $v < v_c$ is generally interpreted as thermally activated creep [3,7–10], the increase of τ_s with v above v_c, where softening of the contacts is expected, could be the result of competition between temperature-induced weakening and rate-induced strengthening [10] of material properties (e.g., yield stress [45]).

The mild decrease of τ_r (~10%) reported here is in stark contrast to both recent rupture experiments in Homalite [26] and to rock friction experiments [15–18], where v is imposed. These experiments demonstrated a significant reduction of the friction coefficient (up to an order of magnitude) that was attributed to the same flash heating mechanism. One significant difference with our experiments is that the experiments in rock form a continuous gouge layer of ground rock that is sandwiched between the sliding surfaces. In our experiments no gouge is formed and the interface is always composed of a sparse ensemble of discrete contacts.

Understanding these results is a challenge that could be related to the qualitative character of frictional interfaces. Our experiments present strong evidence that, while flash heating may occur, this mechanism is not, in itself, a necessary condition for strong frictional weakening. The answers could lie in better understanding the complex dynamics of discrete contacts under extreme conditions and slip rates.

We thank E. Bouchbinder, Y. Bar-Sinai, and M. Aldam for fruitful comments. We also acknowledge the support of both the US-Israel Binational Science Foundation (Grant No. 2016950), and Israel Science Foundation (Grant No. 1523/15). E. B. acknowledges the support from the Lady Davis Trust.

[1] F. P. Bowden and D. Tabor, *The Friction and Lubrication of Solids*, 2nd ed. (Oxford Univ. Press, New York, 2001).

[2] J. H. Dieterich and B. D. Kilgore, Tectonophysics **256**, 219 (1996).

[3] T. Baumberger and C. Caroli, Adv. Phys. **55**, 279 (2006).
[4] C. Marone, Annu. Rev. Earth Planetary Sci. **26**, 643 (1998).
[5] T. Baumberger, P. Berthoud, and C. Caroli, Phys. Rev. B **60**, 3928 (1999).
[6] K. Nagata, M. Nakatani, and S. Yoshida, J. Geophys. Res. **117**, B02314 (2012).
[7] M. Nakatani, J. Geophys. Res. **106**, 13347 (2001).
[8] J. R. Rice, N. Lapusta, and K. Ranjith, J. Mech. Phys. Solids **49**, 1865 (2001).
[9] T. Putelat, J. H. Dawes, and J. R. Willis, J. Mech. Phys. Solids **59**, 1062 (2011).
[10] Y. Bar-Sinai, R. Spatschek, E. A. Brener, and E. Bouchbinder, J. Geophys. Res. **119**, 1738 (2014).
[11] B. M. Kaproth and C. Marone, Science **341**, 1229 (2013).
[12] Y. Bar-Sinai, R. Spatschek, E. A. Brener, and E. Bouchbinder, Phys. Rev. E **88**, 060403 (2013).
[13] J. C. Chang, D. A. Lockner, and Z. Reches, Science **338**, 101 (2012).
[14] J. R. Rice, J. Geophys. Res. **111** (2006).
[15] D. L. Goldsby and T. E. Tullis, Science **334**, 216 (2011).
[16] G. Di Toro, R. Han, T. Hirose, N. De Paola, S. Nielsen, K. Mizoguchi, F. Ferri, M. Cocco, and T. Shimamoto, Nature (London) **471**, 494 (2011).
[17] K. M. Brown and Y. Fialko, Nature (London) **488**, 638 (2012).
[18] F. X. Passelègue, D. L. Goldsby, and O. Fabbri, Geophys. Res. Lett. **41**, 828 (2014).
[19] S. M. Rubinstein, G. Cohen, and J. Fineberg, Nature (London) **430**, 1005 (2004).
[20] P. G. Okubo and J. H. Dieterich, J. Geophys. Res. **89**, 5817 (1984).
[21] M. Ohnaka, *The Physics of Rock Failure and Earthquakes*, 1st ed. (Cambridge University Press, New York, 2013).
[22] M. Mello, H. S. Bhat, and A. J. Rosakis, J. Mech. Phys. Solids **93**, 153 (2016).
[23] O. Ben-David, S. M. Rubinstein, and J. Fineberg, Nature (London) **463**, 76 (2010).
[24] I. Svetlizky and J. Fineberg, Nature (London) **509**, 205 (2014).
[25] F. X. Passelègue, A. Schubnel, S. Nielsen, H. S. Bhat, D. Deldicque, and R. Madariaga, J. Geophys. Res. **121**, 4343 (2016).
[26] V. Rubino, A. Rosakis, and N. Lapusta [Nature Commun. (to be published)].
[27] I. Svetlizky, D. Pino Muñoz, M. Radiguet, D. S. Kammer, J.-F. Molinari, and J. Fineberg, Proc. Natl. Acad. Sci. U.S.A. **113**, 542 (2016).
[28] See Supplemental Material at http://link.aps.org/supplemental/10.1103/PhysRevLett.118.234301 for details of the experimental analysis, measurements of the contact area aging, and estimations of the temperature increase. Included are Refs. [29–31].
[29] O. Ben-David, G. Cohen, and J. Fineberg, Science **330**, 211 (2010).
[30] B. J. Briscoe and K. S. Sebastian, Proc. R. Soc. A **452**, 439 (1996).
[31] P. Berthoud, T. Baumberger, C. G'Sell, and J.-M. Hiver, Phys. Rev. B **59**, 14313 (1999).
[32] S. M. Rubinstein, M. Shay, G. Cohen, and J. Fineberg, Int. J. Fract. **140**, 201 (2006).
[33] I. Svetlizky, D. S. Kammer, E. Bayart, G. Cohen, and J. Fineberg, Phys. Rev. Lett. **118**, 125501 (2017).
[34] H. Shlomai and J. Fineberg, Nat. Commun. **7**, 11787 (2016).
[35] M. Aldam, Y. Bar-Sinai, I. Svetlizky, E. A. Brener, J. Fineberg, and E. Bouchbinder, Phys. Rev. X **6**, 041023 (2016).
[36] B. E. Read and J. C. Duncan, Polymer Testing **2**, 135 (1981).
[37] M. Radiguet, D. S. Kammer, P. Gillet, and J.-F. Molinari, Phys. Rev. Lett. **111**, 164302 (2013).
[38] D. S. Kammer, M. Radiguet, J.-P. Ampuero, and J.-F. Molinari, Tribol. Lett. **57**, 23 (2015).
[39] E. Bayart, I. Svetlizky, and J. Fineberg, Nat. Phys. **12**, 166 (2016).
[40] J. H. Dieterich and B. D. Kilgore, Pure Appl. Geophys. **143**, 283 (1994).
[41] V. Popov, B. Grzemba, J. Starcevic, and C. Fabry, Physical Mesomechanics **13**, 283 (2010).
[42] P. Bhattacharya, A. M. Rubin, E. Bayart, H. M. Savage, and C. Marone, J. Geophys. Res. **120**, 6365 (2015).
[43] A. Cabboi, T. Putelat, and J. Woodhouse, J. Mech. Phys. Solids **92**, 210 (2016).
[44] M. Nakatani and C. H. Scholz, J. Geophys. Res. **111** (2006).
[45] J. Richeton, S. Ahzi, K. Vecchio, F. Jiang, and R. Adharapurapu, Int. J. Solids Struct. **43**, 2318 (2006).